Trans. Korean Soc. Noise Vib. Eng., 26(3) : 270~280, 2016
http://dx.doi.org/10.5050/KSNVE.2016.26.3.270

한국소음진동공학회논문집 제 26 권 제 3 호, pp. 270~280, 2016
ISSN 1598-2785(Print), ISSN 2287-5476(Online)

The Evolution of Electromechanical Admittance from Mode-converted Lamb Waves Reverberating on a Notched Beam

노치가 있는 보에서 잔향하는 모드변환 램파의 전기역학적 어드미턴스 전이

Eun Jin Kim* and Hyun Woo Park†
김 은 진·박 현 우

(Received March 3, 2016 ; Revised May 13, 2016 ; Accepted May 13, 2016)

Key Words : Mode-converted Lamb Waves(모드변환된 램파), Temporal Spectrum(템포럴 스펙트럼), Beam(보), Notch(노치), Finite Element Analysis(유한요소 해석), Piezoelectric(PZT) Wafer(압전박막), Truncation Time(절단시간), Root Mean Square(제곱평균제곱근), Fast Fourier Transform(고속 푸리에 변환), Wave Propagation Perspective(파전달 관점)

ABSTRACT

This paper investigates the evolution of EM admittance of piezoelectric transducers mounted on a notched beam from wave propagation perspective. A finite element analysis is adopted to obtain numerical solutions for Lamb waves reverberating on the notched beam. The mode-converted Lamb wave signals due to a notch are extracted by using the polarization characteristics of piezoelectric transducers collocated on the beam. Then, a series of temporal spectrums are computed to demonstrate the evolution of EM admittance through fast Fourier transform of the mode-converted Lamb wave signals which are consecutively truncated in the time domain. When truncation time is relatively small, the corresponding temporal spectrum is governed by the characteristics of the input driving frequency. As truncation time becomes large, however, the modal characteristics of the notched beam play a crucial role in the temporal spectrum within the input driving frequency band. This implies that mode-converted Lamb waves reverberating on the beam contributes to the resonance of the beam. The root mean square values are computed for the temporal spectrums in the vicinity of each resonance frequency. The root mean square values increase monotonically with respect to truncation time for any resonance frequencies. Finally the implications of the numerical observation are discussed in the context of damage detection of a beam.

요 약

노치가 있는 보에 부착된 압전소자의 전기역학적 어드미턴스 전이과정을 파전달 관점에서 규명한다. 유한요소 해석을 통해 노치가 있는 보에서 잔향하는 램파에 대한 수치해를 구한다. 보에 병치된 압전소자의

† Corresponding Author; Member, Dept. of Civil Engineering, Dong-A Univ.
E-mail: hwpark@donga.ac.kr
* Road Facility Management Division, Seoul Metropolitan Facilities Management Corporation

‡ Recommended by Editor Hyung Jo Jung

분극을 이용하여 노치에 의해 발생하는 모드변환된 램파 신호를 추출한다. 전기역학적 어드미턴스의 전이 과정을 보여줄 수 있는 일련의 템포럴 스펙트럼은 모드변환된 램파 신호들을 시간영역에서 순차적으로 절단한 후, 고속 푸리에 변환을 적용하여 계산한다. 절단 시간이 상대적으로 작을 때 이에 대응되는 템포럴 스펙트럼은 입력 주파수 대역의 특성이 지배적이다. 그러나, 절단 시간이 증가함에 따라 입력 주파수 대역 내에 존재하는 보의 모달 특성이 템포럴 스펙트럼에 중대한 영향을 준다. 이는 보에서 잔향하는 모드변환 램파가 보의 공진에 기여함을 의미한다. 각 공진주파수 부근에서 템포럴 스펙트럼에 대한 제곱평균제곱근을 계산한다. 모든 공진주파수 부근에서 절단시간에 따라 제곱평균제곱근은 증가한다. 마지막으로, 보의 손상 진단 측면에서 수치해석 결과의 시사점에 대해 논의한다.

1. Introduction

Lamb wave and electro-mechanical (EM) impedance signals have been widely used for damage detection for a beam using PZT transducers[1,2]. Although Lamb wave and EM impedance signals are created and received through a single PZT configuration, Lamb wave and EM impedance signals have been dealt with independently in the previous damage detection schemes so far due to their own merits. The Lamb waves are suitable for a far-field damage detection because they can travel a long distance on a beam[1,3,4]. On the other hand, EM impedance signatures are advantageous for a near-field damage detection because they are known to mainly interact with damage in the vicinity of PZT[2,5~7]. Some researchers attempt to combine the Lamb wave and EM impedance approaches for the synergistic use of their complementary merits[8~10]. However, there have been few theoretical researches on the underlying relations between the Lamb wave and EM impedance signals. Recently, Park has analytically investigated the evolution of EM admittance (an inverse of EM impedance) of PZTs mounted on an intact beam from a wave propagation perspective[11]. The analytical investigation has provided a rigorous insight on the theoretical relevance between guided waves and EM admittance.

This paper investigates the evolution of EM admittance on a notched beam from a wave propagation perspective. In particular, the underlying relevance will be studied between the EM admittance and the mode-converted Lamb wave signals induced by a notch on beam. Because the analytic wave solutions are difficult to derive for Lamb waves reverberating on a notched beam, a finite element analysis is utilized to obtain numerical solutions. Using the polarization characteristics of PZT collocated on a beam, the mode-converted Lamb wave signals are extracted. The evolution of EM admittance is demonstrated through temporal spectrums of the mode-converted Lamb waves. The temporal spectrums are computed through fast Fourier transform with increasing truncation time windows. The convergence of the temporal spectrums to EM admittance with respect to truncation time is presented, producing the resonance of the beam. The root mean square (RMS) values of the temporal spectrums are calculated with respect to truncation time. Finally the implications of the numerical observation are discussed in the context of damage detection of a beam.

2. Temporal spectrums of Lamb wave signals: relevance of Lamb wave propagation to vibration modes of a beam

Both Lamb wave and vibration of a plate can be easily generated and measured through the EM coupling between the PZT wafers and the structure. Figure 1 schematically illustrates how Lamb waves induced by PZT wafers converge to the resonant state. In Fig. 1(a), a cantilever beam with collocated PZT wafers is presented for the

simplicity of explanation. This cantilever beam model has been first utilized in the experimental work of the authors[6]. Finite element analysis using ABAQUS 6.7-4 standard[12] is conducted to obtain the Lamb wave mode signals generated and received by PZT wafers in the time domain. Detailed description can be found in the previous works by the authors regarding mesh layout and finite element types for the PZT-beam system used in the numerical simulation[13]. As harmonic excitations of the 11th natural mode shape (f = 15.4 kHz) are applied to the PZT wafers, Lamb waves begin to propagate from the actuating PZT wafers as shown in Fig. 1(c). Then, incident Lamb waves and reflections from the boundaries of the beam are superimposed, producing transient dynamic states in Fig. 1(d).

A temporal spectrum is employed to investigate the convergence of Lamb wave motions to the vibration response of a beam in the frequency domain:

$$\hat{V}(\omega,T)=\int_{-\infty}^{\infty}\{H(t)-H(t-T)\}V(t)e^{-i\omega t}dt \qquad (1)$$

where t, ω, T, $H(t)$ and $V(t)$ are time, angular frequency, truncation time, a Heaviside step function and Lamb wave mode signals captured by a PZT wafer, respectively. As truncation time T increases, more and more reflected Lamb wave mode signals will participate in the temporal spectrum. If T approaches infinite, Eq. (1) becomes identical to Fourier transform of Lamb wave mode signals with an infinite number of reflections at the boundaries of a beam. Therefore, we can investigate the effects of wave reflections on the temporal spectrum by increasing the truncation time.

Temporal spectrums of the cantilever beam with increasing truncation time are demonstrated in Fig. 2. Since Fast Fourier transform (FFT) is used to compute temporal spectrums, the number of sampled Lamb wave mode signals is set to be n power of 2. The nth truncation time T_n becomes

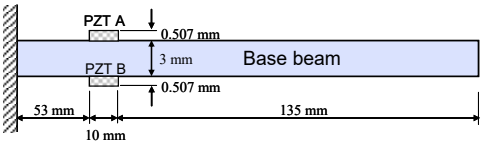

(a) A cantilever beam with two collocated PZTs

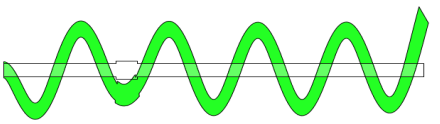

(b) Natural mode shape at 15.4 kHz

(c) Initial wave propagation produced by a harmonic excitation at 15.4 kHz(t = 12 ms)

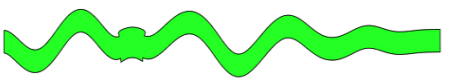

(d) Transient state (t = 75 ms)

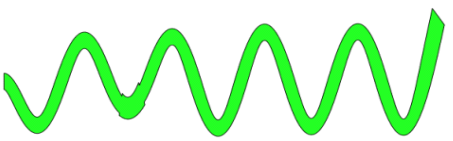

(e) Resonant state (t = 624 ms)

Fig. 1 Convergence of transient Lamb waves to resonant standing waves with a harmonic excitation of the collocated PZTs at one of the resonance frequencies: (a) A schematic of a cantilever beam with two collocated PZTs; (b) The 11th natural mode shape computed by eigenvalue analysis; (c) Initial Lamb wave propagation induced by the harmonic excitation of the collocated PZTs at the 11th natural frequency of the beam; (d) Superposition of incident Lamb waves and reflections, (e) Constructive superposition of incident and reflective Lamb waves produce resonant standing waves identical to the natural mode shape in (b)[13] (©IOP Publishing. Reproduced with permission. All rights reserved)

$2^{(n+6)}\Delta t$ where sampling interval t = 0.25 s. Four temporal spectrums are compared in Fig. 2(b). As the truncation time increases, the peaks of the temporal spectrums in Fig. 2(d) begin to appear near the resonance frequency (11th mode, f = 15.4 kHz).

From now on, temporal spectrums of Lamb wave

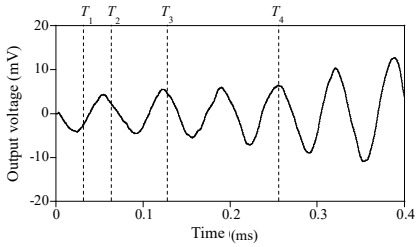

(a) Truncation times ($T_1 \sim T_4$ = 0.032 ms ~ 0.256 ms) to compute temporal spectrums of initial Lamb wave mode signals when the harmonic input signal is imposed on PZT A

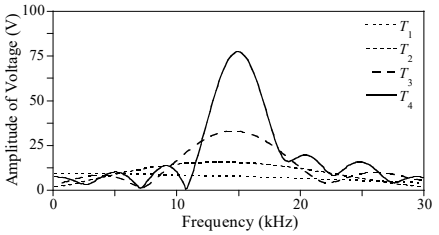

(b) Temporal spectrums of Lamb wave mode signals for truncation times $T_1 \sim T_4$ in (a)

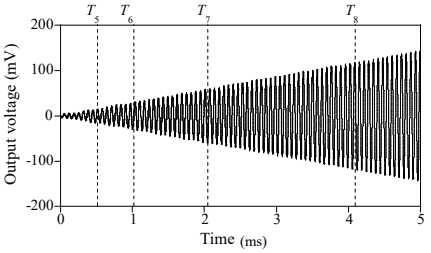

(c) Truncation times ($T_5 \sim T_8$ = 0.512 ms ~ 4.096 ms) to compute temporal spectrums of Lamb wave mode signals when the harmonic input signal is imposed on PZT A

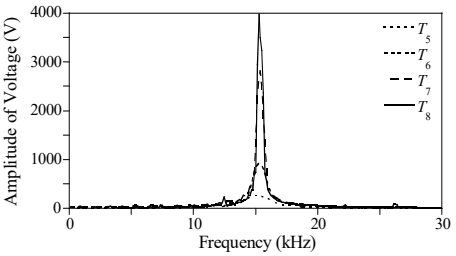

(d) Temporal spectrums of Lamb wave mode signals for truncation times $T_5 \sim T_8$ in (c)

Fig. 2 Temporal spectrums of Lamb wave mode signals for increasing truncation times when the harmonic input signal is imposed on PZT A at the 11th natural frequency of the cantilever beam in Fig. 2(a)

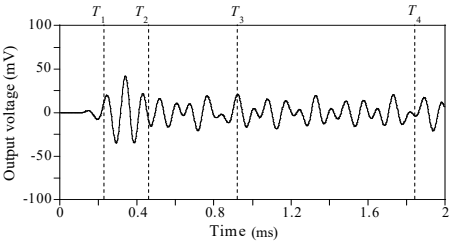

(a) Truncation times ($T_1 \sim T_4$ = 0.230 ms ~ 1.843 ms) to compute temporal spectrums of initial Lamb wave mode signals when the 10 kHz tone-burst input signal is imposed on PZT

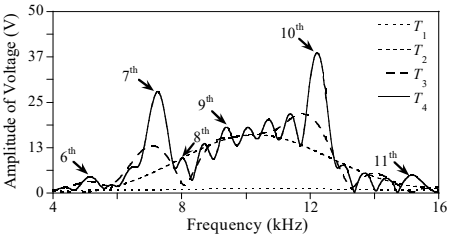

(b) Temporal spectrums of Lamb wave mode signals for $T_1 \sim T_4$ in (a)

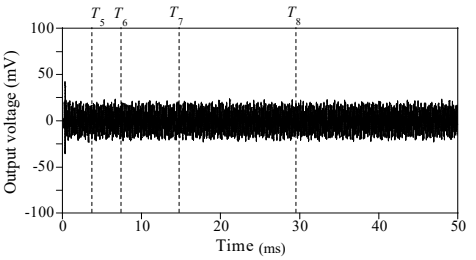

(c) Truncation times ($T_5 \sim T_8$ = 3.686 ms ~ 29.491 ms) to compute temporal spectrums of Lamb wave mode signals when 10 kHz tone burst input signal is imposed on PZT A

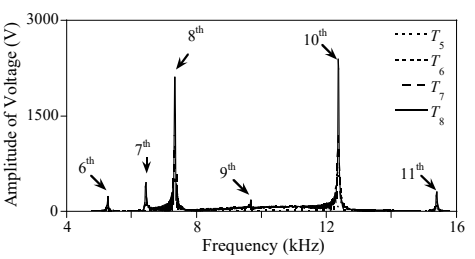

(d) Temporal spectrums of Lamb wave mode signals for $T_5 \sim T_8$ in (c)

Fig. 3 Temporal spectrums of Lamb wave mode signals for increasing truncation times when 10 kHz tone burst input signal is imposed on PZT A of a cantilever beam in Fig. 2(a)

mode signals are investigated in case of a tone-burst input that is widely used in Lamb wave based damage detection. Numerical simulation through finite element analysis is conducted in the same way as the harmonic input excitation case. A tone burst input with 10 kHz center frequency is applied to PZT A in Fig. 1(a) and the corresponding response signals are measured from PZT A as well. Similar to Fig. 2, the response Lamb wave mode signals up to 50 ms are truncated with increasing truncation times and temporal spectrums are computed through fast Fourier transform as shown Fig. 3. Here, time interval (Δt) is 1.8 μs and nth truncation time T_n is set to be $2^{(n+6)}\,\Delta t$. All temporal spectrums are demonstrated within the bandwidth of the tone-burst input from 4 to 16 kHz.

The shape of the temporal spectrum for T_1 is almost identical to that of the power spectrum of the tone-burst input signal in Fig. 3(b). As truncation time increases from T_2 to T_4, several peaks begin to appear gradually in temporal spectrums. As truncation time increases from T_5 to T_8 as shown in Fig. 3(c), peaks in temporal spectrums become sharper and the corresponding frequencies converge to the natural frequencies of the cantilever beam as shown in Fig. 3(d).

When truncation time is sufficiently large, e.g. $T_8 = 29.491$ ms, the associated temporal spectrum asymptotically converges to the electro-mechanical (EM) admittance of PZT A which is used in EM-impedance based damage diagnosis. It is noteworthy that the interested readers can refer to the previous work[11] regarding the detailed analytical description between temporal spectrums and the EM admittance from wave propagation perspective for the tone-burst input excitation.

3. Decomposition of Lamb wave mode signals

Mode conversion occurs when Lamb waves propagating along a thin beam encounter a discontinuity point such as crack[3]. For example, when the first symmetric Lamb wave mode (S_0) encounters the discontinuity, the transmitted wave is separated into fundamental symmetric (S_0) and anti-symmetric (A_0) Lamb wave modes (denoted as S_0/S_0 and A_0/S_0, respectively). In a similar fashion, an A_0 mode produces S_0 and A_0 modes (S_0/A_0 and A_0/A_0)[13].

Using two identical PZT wafers collocated on both sides of a beam, each individual Lamb wave modes can be extracted through selective excitation and sensing of the PZT wafers[14]. Figure 4 demonstrates a schematic in which each individual

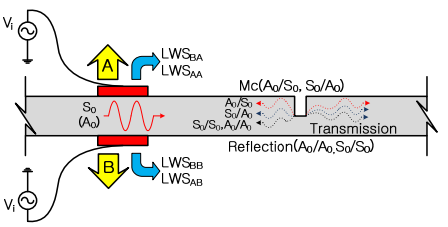

(a) Extraction of LWS with collocated PZT wafers as an actuator and a sensor alternately

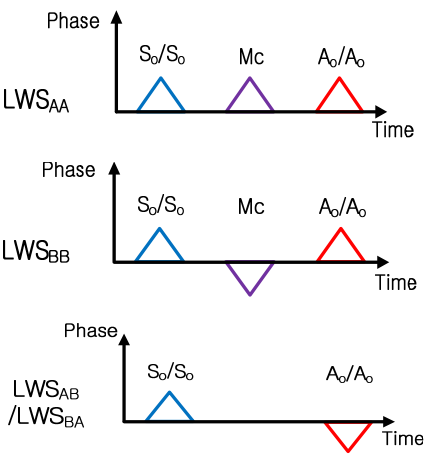

(b) Relative phase information in LWS_{AA}, LWS_{BB}, and $LWS_{AB(/BA)}$ obtained from (a)

Fig. 4 Comparison of relative phase information among LWS_{AA} LWS_{BB} and $LWS_{AB(/BA)}$ obtained from collocated PZT wafers. Note that it is assumed that only A_0 and S_0 Lamb wave mode existand the S_0 mode propagates faster than the A_0 mode

Lamb wave mode can be isolated through the collocated PZT wafers for a pulse-echo method. The arrows over and under PZT A and B indicate the poling directionalities of the PZT wafers. LWS stands for Lamb wave mode signal while the first and second subscripts of LWS denote the actuating and sensing PZT, respectively.

For the simplicity of description, only S_0 and A_0 Lamb wave modes are considered, and S_0 mode is assumed to travel faster than A_0 mode. In this case, the first arrivals of the converted modes (S_0/A_0 and A_0/S_0) appear between the first arrivals of the S_0 and A_0 modes reflected from the notch. Because the waveforms and the arrival times of S_0/A_0 and A_0/S_0 modes are exactly same except the phase difference by π radian, the S_0/A_0 and A_0/S_0 modes appear in LWS_{AA} and LWS_{BB} while they cancel out in LWS_{AB} and LWS_{BA} due to the poling directionalities of PZT A and B[13].

Using the relative phase differences of LWS_{AA}, LWS_{BB} and LWS_{AB} each Lamb wave mode can be isolated through the following algebraic equation[13]:

$$\begin{Bmatrix} LWS_{AA}(t) \\ LWS_{BB}(t) \\ LWS_{AB}(t) \end{Bmatrix} = \begin{bmatrix} 1 & 1 & 1 \\ 1 & -1 & 1 \\ 1 & 0 & -1 \end{bmatrix} \begin{Bmatrix} LWS_{S_0}(t) \\ LWS_{MC}(t) \\ LWS_{A_0}(t) \end{Bmatrix} \tag{2}$$

where subscripts S_0, MC and A_0 of LWS denote isolated S_0, mode-converted (S_0/A_0 or A_0/S_0) and A_0 Lamb wave modes, respectively.

Having said the signal decomposition of Lamb wave mode signals associated with mode conversion, it is possible to apply the same signal decomposition to the temporal spectrums of Lamb wave mode signals for any truncation times. If truncation time is large enough, for example, the signal decomposition for Lamb wave mode signals can be extended to EM signals because the temporal spectrum can represent the EM impedance or admittance. More specifically, EMS_{ij} represents an EM signal being a frequency response function at the *i*'th sensing PZT when an input driving voltage I is applied to the *j*'th PZT wafer as follows:

$$EMS_{ij}(\omega) = \Im[LWS_{ij}(t)] / \Im[I(t)] \tag{3}$$

where, $\Im[\cdot]$ stands for Fourier transform operator, LWS_{ij} is the Lamb wave mode signal at the *i*'th PZT corresponding to an input at the *j*'th PZT, and ω is an angular frequency.

Using Eqs. (2) and (3), the decomposed EM signals corresponding to each Lamb wave mode can be obtained[13]:

$$\begin{bmatrix} EMS_{S_0} \\ EMS_{MC} \\ EMS_{A_0} \end{bmatrix} = \begin{bmatrix} 1 & 1 & 1 \\ 1 & -1 & 1 \\ -1 & 0 & 1 \end{bmatrix}^{-1} \begin{bmatrix} EMS_{AA} \\ EMS_{BB} \\ EMS_{AB} \end{bmatrix} \tag{4}$$

4. Temporal spectrums of mode-converted Lamb wave signals reverberating on a notched beam

In this subsection, the temporal spectrums of Lamb wave mode signals reverberating on a notched beam is investigated when a harmonic input signal is applied to the collocated PZT wafers. The mode-converted Lamb wave signals can be extracted using Eq. (2). Detailed description on the circuit layout of the collocated PZT wafers and the geometric configuration of the beam with a notch are illustrated in Figs. 5(a) and (b), respectively. The location of the notch has been assigned arbitrarily near the middle of the cantilever beam. The notch size is as small as an individual finite element (1 mm × 1 mm) of the beam. The notch can be numerically simulated by removing a single finite element at the notch location from an intact beam model. Because the analytic wave solutions are difficult to derive for the scattered Lamb waves on a notched beam, finite element analysis (ABAQUS 6.7-4 standard)[12] has been used to obtain Lamb wave mode signals in the time domain.

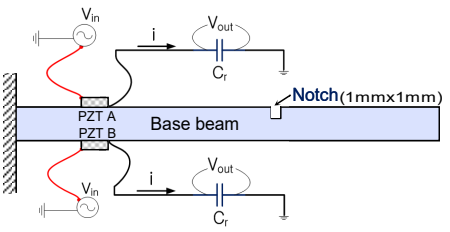

(a) Actuating and sensing circuit layouts for identical PZT wafers collocated on a cantilever beam with a notch

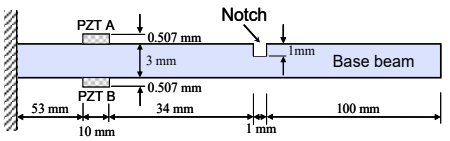

(b) Geometric configuration of a cantilever beam with a notch and PZT wafers collocated on the beam

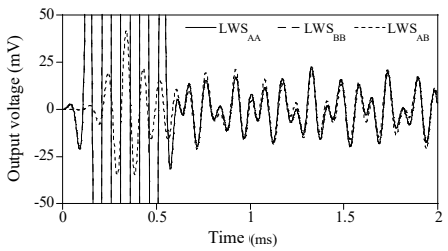

(c) Lamb wave mode signals measured from the intact cantilever beam

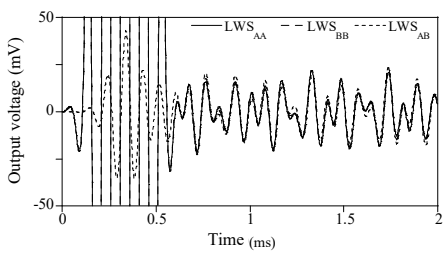

(d) Lamb wave mode signals measured from the damaged cantilever beam

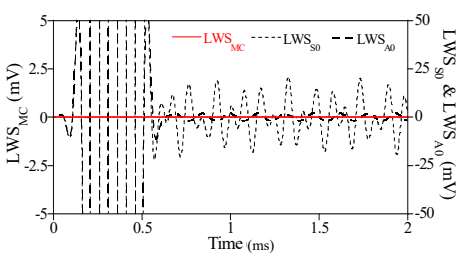

(e) Decomposed Lamb wave mode signals of the intact cantilever beam

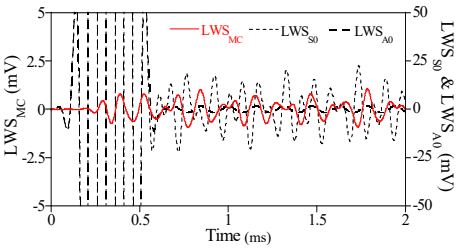

(f) Decomposed Lamb wave mode signals of the damaged cantilever beam

Fig. 5 Decomposition of the Lamb wave mode signals measured from the intact and damaged conditions of the cantilever beam when tone burst input with 10 kHz center frequency are applied. The capacitance values of the both self-sensing circuits are kept the same (3nF)

10 kHz tone burst input signal is applied for investigating the temporal spectrums of mode-converted Lamb wave signals reverberating on the notched beam. Lamb wave mode signals are generated and received by a pair of PZT wafers on an intact and damaged cantilever beams in Figs. 1(a) and 5(b). Because the attached PZT wafers on the two beams can act as an actuator, the free surface of each collocated PZT wafer gets connected to a voltage source (V_{in}). The other surface of each PZT wafer is tied to a sensing circuit consisting of a single capacitor ($C_r = 3nF$) at the same time and the output voltage (V_{out}) is measured at the sensing circuit as shown in Fig. 5(a) for both intact and notched beams. Lamb wave mode signals measured from the intact and damaged beam conditions are presented in Fig. 5(c) and (d), respectively. LWS_{AA} and LWS_{BB} have both piezoelectric and dielectric components while LWS_{AB} contains the piezoelectric component only. The piezoelectric component in LWS_{AA} and LWS_{BB} is often masked by the large magnitude of the dielectric component and thus is not clearly observed in Figs. 5(c) and (d)[13]. On the other hand, the piezoelectric component is clearly observed in LWS_{AB} displaying the resonant characteristics of the beam. LWS_{S0}, LWS_{A0} and LWS_{MC}

decomposed from LWS_{AA}, LWS_{BB} and LWS_{AB} by using Eq. (2) are shown in Figs. 5(e) and (f), respectively. Note that LWS_{MC} in Fig. 5(e) is a null signal because no mode conversion occurs in the intact cantilever beam. On the other hand, LWS_{MC} in Fig. 5(f) is observed clearly due to the mode conversion in the damaged beam.

Fig. 6(a) presents LWS_{MC} in Fig. 5(f) scaled up to 2.0 ms and truncation times for computing the temporal spectrums of LWS_{MC}. Here, the truncation times are identical to those adopted in Fig. 3(a). The peak of the temporal spectrum for T_2 is located in the vicinity of 10 kHz which is the driving frequency of the tone-burst input in Fig. 6(b). As truncation time increases from T_2 to T_4, several peaks begin to appear gradually and their amplitude increases in the temporal spectrums similar to Fig. 3(b). This implies that mode converted Lamb waves induced by the notch participate in the vibration modes of the cantilever beam step by step as truncation time increases. Fig. 6(c) demonstrates LWS_{MC} scaled up to 50 ms and truncation times which are identical to those in Fig. 3(c). As truncation time increases from T_5 to T_8, peaks in temporal spectrums surges up and the corresponding frequencies converge to the natural frequencies of the cantilever beam as shown in Fig. 3(d).

The RMS values of temporal spectrums for LWS_{MC} with respect to truncation time are demonstrated in Fig. 7. Here, the RMS of a temporal spectrum $\hat{V}(\omega,T)$ is defined as the following equation:

$$RMS[\hat{V}(\omega,T)] = \sqrt{\int_{\omega_0}^{\omega_1} \left|\hat{V}(\omega,T)\right|^2 dx \Big/ (\omega_1 - \omega_0)} \qquad (5)$$

where ω_0 and ω_1 determine an interval to integrate the temporal spectrum.

In Fig. 7(a), RMS values of temporal spectrums associated with individual modes (6th ~ 11th) are presented with respect to truncation time. The

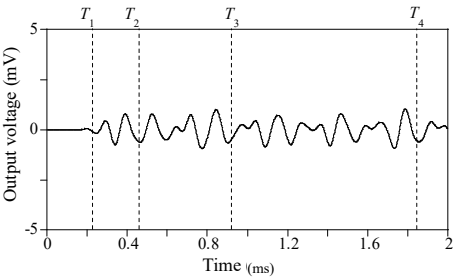

(a) Truncation times ($T_1 \sim T_4 = 0.230$ ms ~ 1.843 ms) to compute temporal spectrums of initial LWS_{MC} when the 10 kHz tone-burst input signal is imposed

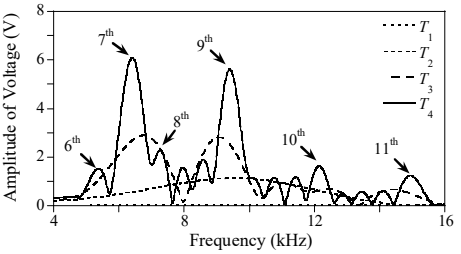

(b) Temporal spectrums of LWS_{MC} for $T_1 \sim T_4$ in Fig. 6(a)

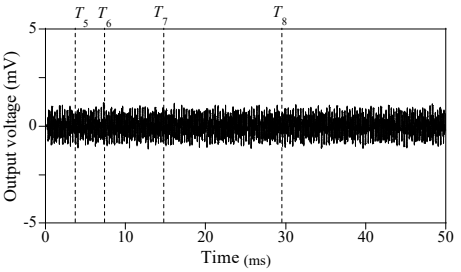

(c) Truncation times ($T_5 \sim T_8 = 3.686$ ms ~ 29.491 ms) to compute temporal spectrums of LWS_{MC} when 10 kHz tone burst input signal is imposed

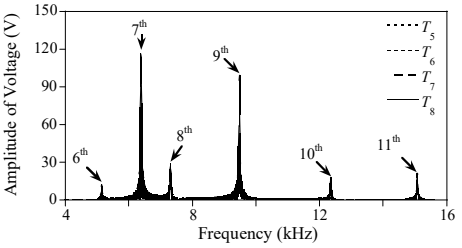

(d) Temporal spectrums of LWS_{MC} for $T_5 \sim T_8$ in Fig. 6(c)

Fig. 6 Temporal spectrums of LWS_{MC} for increasing truncation times when the 10 kHz tone burst input signal is imposed in the cantilever beam with a notch in Fig. 5(b)

integration interval for the RMS value of the temporal spectrum is from $0.9\omega_n$ to $1.1\omega_n$ where ω_n is the nth natural frequency. Note that all RMS values for the individual modes monotonically increase with truncation time increasing as shown in Fig. 7(a). The increasing trend of each RMS value in Fig. 7(a) is closely related to the modal characteristics of the locations of both the PZTs and the notch. For example, if the PZTs and the damage are on the node of a certain modal strain, it is likely that the corresponding RMS value will increase very slowly with respect to truncation time. If both are on the anti-nodes of modal strain, the associated RMS value increases very rapidly. We have conducted several numerical simulations for different locations of PZTs and the notch. The RMS values of individual modes increase monotonically in any cases. This implies that the S/N ratio associated with the mode-converted Lamb wave signal due to the notch is improved through the resonance behavior of a structure regardless of the modal characteristics of the structure. Fig. 7(b) demonstrates the RMS values of the overall temporal spectrum with respect to truncation time. The integration interval for the RMS values is from 4 kHz to 16 kHz which is the bandwidth of the input tone burst input. Because RMS values associated with each mode increases with respect to truncation time, the RMS values of the overall temporal spectrum increases behaves exactly same as well.

Three implications can be drawn from Fig. 7 in the context of reference-free damage detection of a beam. First, any RMS values of temporal spectrums for LWS_{MC} can be a good damage index for reference-free damage detection of a beam because they should become zeros if no damage exists on a beam. Second, damage detectability can be significantly improved by increasing truncation time since signal-to-noise ratio of the damage index is enhanced monotonically as truncation time increases. The temporal spectrum approaches the EM admittance curve through the participation of mode converted Lamb waves to the resonance of a damaged beam as truncation time goes to infinite. This implies that the EM admittance-based (or impedance-based) method may be combined with Lamb-wave based approach because they can be realized through a single configuration of PZTs. Third, the RMS value for an overall temporal spectrum including several modes is more appropriate for damage index than those for temporal spectrum associated with an individual mode. In other words, the risk of choosing a local mode insensitive to given damage and PZT locations can be avoided effectively by including several modes to compute the RMS value of the temporal spectrum.

In case of a complex waveguide such as a beam with stiffeners, the mode-converted Lamb wave signals due to damage are difficult to extract through the Lamb wave decomposition described in Section 3. This is because both stiffener and

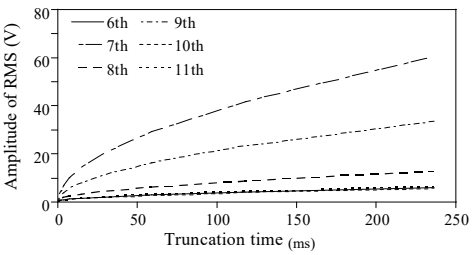

(a) RMS values of temporal spectrums for LWS_{MC} associated with individual modes

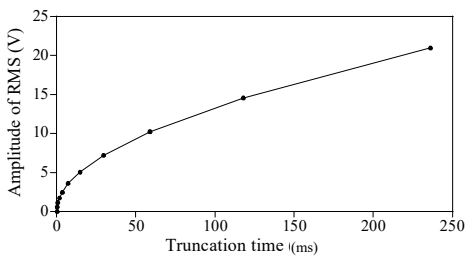

(b) RMS values of temporal spectrums for LWSMC associated with overall modes

Fig. 7 RMS values of temporal spectrums for LWS_{MC} in Fig. 6

damage may create mode-converted Lamb waves at the same time. In this particular case, the baseline Lamb wave signals from an intact structure are needed. The scattered Lamb wave signals purely caused by damage can be extracted by comparing baseline signals and those obtained from a damage structure. Then, the temporal spectrum analysis described in Section 4 will present the evolution of the EM admittance from the scattered Lamb wave signals reverberating on the host structure.

5. Conclusion

This paper investigates the evolution of EM admittance on a notched beam from a wave propagation perspective for a tone-burst input excitation. The polarization characteristics of collocated PZT wafers on both side of beam enables extracting mode-converted Lamb wave signal induced by the notch reverberating on the beam. First, finite element analysis is performed to obtain the mode-converted Lamb wave signal, and then a series of temporal spectrums is computed through the fast Fourier transform of the mode-converted Lamb wave signals with respect to truncation time. When truncation time is relatively small, the corresponding temporal spectrum is governed by the characteristics of the input driving frequency. As truncation time becomes large, however, the modal characteristics of the beam play a crucial role in the temporal spectrum within the input driving frequency band. This implies that the reverberation of the mode-converted Lamb waves contributes to the resonance of the notched beam. The root mean square values are computed for the temporal spectrums in the vicinity of each resonance frequency. The root mean square values increase monotonically with respect to truncation time regardless of resonance frequencies.

It is shown that the temporal spectrum approaches the EM admittance curve through the participation of mode converted Lamb waves to the resonance of a notched beam as truncation time goes to infinite. This implies that the EM admittance-based (or impedance-based) method may be combined with Lamb-wave based approach because they can be realized through a single configuration of PZTs. The risk of choosing a local mode insensitive to given damage and PZT locations can be avoided effectively by including several modes to compute the root mean value of the temporal spectrum.

References

(1) Raghavan, A. and Cesnik, C. E. S., 2007, Review of Guided-wave Structural Health Monitoring, The Shock and Vibration Digest, Vol. 39, No. 91, pp. 91~114.

(2) Park, G., Sohn, H., Farrar, C. R. and Inman, D. J., 2003, Overview of Piezoelectric Impedance-based Health Monitoring and Path Forward, The Shock and Vibration Digest, Vol. 35, No. 6, pp. 451~463.

(3) Alleyne, D. N. and Cawley, P., 1992, The Interaction of Lamb Waves with Defects. IEEE Transactions on Ultrasonic, Ferroelectrics and Frequency Control, Vol. 39, No. 3, pp. 381~387.

(4) Cawley, P. and Alleyne, D., 1996, The Use of Lamb Wave for the Long Range Inspection of Large Structures, Ultrasonics, Vol. 34, No. 2, pp. 287~290.

(5) Annamdas, V. G. M. and Soh, C. K., 2010, Application of Electromechanical Impedance Technique for Engineering Structures: Review and Future Issues, Journal of Intelligent Material Systems and Structures, Vol. 21, No. 1, pp. 41~59.

(6) Kim, E. J., Sohn, H. and Park, H. W., 2009, Experimental Verification of Spectral Element Analysis for the High-frequency Responses of a Beam with a Surface Bonded Piezoelectric Transducer, Transaction of Korean Society of Noise and Vibration Engineering, Vol. 19, No. 12, pp. 1347~1355.

(7) Giurgiutiu, V. and Zagrai, A., 2002, Embedded Self-sensing Piezoelectric Active Sensors for On-line Structural Identification, Journal of Vibration and Acoustics, Vol. 124, No. 1, pp. 116~125.

(8) Park, S., Yun, C. B., Roh, Y. and Lee, J. J., 2006, PZT-based Active Damage Detection Techniques for Steel Bridge Components, Smart Materials Structures, Vol. 15, No. 4, pp. 957~966.

(9) Thien, A. B., Chiamori, H. C., Ching, J. T., Wait, J. R. and Park, G., 2008, The Use of Macro-fiber Composites for Pipeline Structural Health Assessment. Structural Control and Health Monitoring, Vol. 15, No. 1, pp. 43~63.

(10) An, Y. and Sohn, H., 2012, Integrated Impedance and Guided Wave Based Damage Detection, Mechanical Systems and Signal Processing, Vol. 28, pp. 50~62.

(11) Park, H. W., 2014, Understanding the Electro-mechanical Admittance of Piezoelectric Transducers Collocated on a Finite Beam from the Perspective of Wave Propagation, Journal of Intelligent Material Systems and Structures, Vol. 25, No. 17, pp. 2122~2140.

(12) Abaqus, [User's Manual, Version 6.7], HKS Inc., Providence, Rhode Island.

(13) Kim, E. J., Kim, M. K., Sohn, H. and Park, H. W., 2011, Investigating Electro-mechanical Signals from Collocated Piezoelectric Wafers for the Reference-free Damage Diagnosis of a Plate, Smart Materials and Systems, Vol. 20, No. 6, pp. 065001.

(14) Kim, S. B. and Sohn, H., 2007, Instantaneous Reference-free Crack Detection based on Polarization Characteristics of Piezoelectric Materials, Smart Materials and Structures, Vol. 16, No. 6, pp. 2375~2387.

Eun Jin Kim, his current work is supervision and management of road facilities such as bridges, tunnels and underpass on the motorways in Seoul metropolitan area. The title of his Ph.D. thesis is “Elasto-dynamic Interpretation of a Coupled PZT Beam System for Reference-free Damage Detection of a Plate”.

Hyun Woo Park, his recent research interest is analytical and numerical investigation of electro-mechanical admittance of piezoelectric transducers mounted on a beam from wave propagation perspective. He is interested in investigating the change of vibration characteristics due to crack in a beam from wave propagation perspective as well.